11th World Congress on Computational Mechanics (WCCM XI)
5th European Conference on Computational Mechanics (ECCM V)
6th European Conference on Computational Fluid Dynamics (ECFD VI)
E. Oñate, J. Oliver and A. Huerta (Eds)

A FREE SURFACE MODEL FOR THE NUMERICAL SIMULATION OF OSCILLATING WATER COLUMN SYSTEMS

Schillaci E.[1], **Balcazar N.**[1], **Jofre L.**[1], **Lehmkuhl O.**[1,2], **Castro J.**[1]

[1] Heat and Mass Transfer Technological Center (CTTC), Universitat Politècnica de Catalunya (UPC), ETSEIAT, Colom 11, 08222 Terrassa (Barcelona), Spain. E-mail: cttc@cttc.upc.edu
[2] Termo Fluids, S.L., Avda Jacquard 97 1-E, 08222 Terrassa (Barcelona), Spain. E-mail: termofluids@termofluids.com

Key words: Oscillating Water Column, Conservative Level-Set, Multiphase Flow.

Abstract. The aim of this work is to propose and validate a numerical model that represents the hydrodynamic behavior of an Oscillating Water Column (OWC) device, that has been shown to be one of the most promising ways to extract energy from ocean waves: successful demonstrative set-up have been realized both on shore based structures (LIMPET device in Scotland and PICO plant in Azores) and on anchored floating ones (OE Buoy in Ireland) [1]. A Level Set scheme was employed to track the free moving interface in an incompressible, transient two-phase flow, globally governed by the Navier-Stokes and the mass conservation equations. After being validated, the model was used to investigate the interaction of linear waves with a submerged air chamber; several set-up were analyzed by monitoring the characteristics magnitudes, in order to assess the accuracy of the model and to optimize the hydrodynamic efficiency of the device. In the second part, a single phase Level Set method was developed and used to simulate the same problem.

1 Introduction

An Oscillating Water Column (OWC) device consists of a semi-submerged air chamber, partially filled by sea water and connected to a bidirectional Wells air turbine by means of an air duct. The surface of the water that fills the stucture is made to oscillate by the waves slamming on the outside of the OWC structure, thus acting as a piston that pulls the air into the turbine when the water level is rising, or sucking it when the level is going down; due to its property of rotating always in the same direction, the turbine is able to produce energy continuously.

In this work, the OWC device has been represented as a semi-submerged structure that confines an air quantity (as showed in Figure 1 - left); it is opened to the environment by means of a small orifice that expulses or sucks air when the water surface is moving and whose aim is to model the viscous damping due to the power extraction system. This set-up can constitute an effective way of representing the physical behavior of the device, as demonstrated firstly

by Evans [2], who used potential theory to consider a rectangular OWC in terms of the width of the interior chamber and submergence depth of the front wall but neglecting the viscous effects; hence, he gave an ideal upper limit to the equipment efficiency. Recently, Morris [3] realized some practical tests on OWC models, thus giving a wide experimental reference on OWC performance, by focusing particularly on the influence of front wall geometry.

Some of the latest attempts of simulating these devices by means of numerical models have been done by Zhang [4], that used a Level Set immersed boundary method to simulate the multi-phase physics of the problem, and by Teixeira [5], that used a code based on a semi-implicit two-step Taylor-Galerkin method. Both of them analyzed the hydrodynamic characteristics of the device on a wide range of geometrical parameters.

In this paper, we firstly used a robust conservative Level Set method to simulate the incompressible two phase flow motion and its interaction with the power extraction system; then, we did an attempt to simulate the single liquid phase, thus reducing consistently the computational cost of the simulation. The method consists in deactivating the air phase and extends velocity and pressure fields over the interface, that will be advected according to Level Set or Volume-of-Fluids methods. Similar attemps were done recently by [6] and [7] on different test cases.

Figure 1: (left) Snapshot of the domain used for the simulations. (right) High velocity of the air through the orifice.

2 Numerical model

2.1 Two phase Level Set

A Conservative Level-Set scheme (CLS) [8] was employed to track the free moving interface in an incompressible, transient two-phase flow. The CLS method avoids the loss of mass that happens in Standard Level Set (SLS) methods; however, it complicates the calculation of geometric properties at the interface. The flow is globally governed by the Navier-Stokes equation and the mass conservation equation ($\nabla \cdot \mathbf{u} = 0$), valid in a domain occupied by two incompressible fluids separated by an interface Λ:

$$\frac{\partial \rho \mathbf{u}}{\partial t} + \nabla \cdot (\rho \mathbf{u}\mathbf{u}) = \nabla \cdot (\mu(\nabla \mathbf{u} + \nabla^T \mathbf{u})) - \nabla p + \rho g + \sigma \kappa \nabla \phi \tag{1}$$

where u is the velocity, p is the pressure and μ is the dynamic viscosity, σ is the surface tension and κ is the curvature of Λ. The interface is tracked by means of an advection equation, that in a divergence free field can be written as follows:

$$\frac{\partial \phi}{\partial t} + \mathbf{u} \cdot \nabla \phi = 0 \tag{2}$$

where $\phi(\mathbf{x},t)$ is a regularized distance function. The governing equations are discretized over a Cartesian grid, according to a staggered scheme that helps to avoid spurious pressure modes and it is generally stable for multiphase flows [9]; the convective scheme is an *upwind*, that allows to move effectively the interface (the turbulent scales are not affected because the flow is essentially laminar). The time step was calculated according to the classical CFL criteria.

2.2 Single phase Level Set

In multiphase flows with high density ratio, some high pressure gradients could rise at the interface. They propagates from the high density to the low density phase that could be excessively accelerated and lose its divergence; moreover, in the analysis of some problems the treatment of the air phase can be considered useless and only leads to the waste of a big computational memory employed to update gradients, flux limiters and so on. Finally, in the case of using a CFL scheme to update the time step, its value would be only affected by the velocity of the air phase that can be order of magnitudes higher then in the water phase; this high velocity can be caused by the spurious gradient advected from the water phase or simply by the geometrical and physical features of the set-up. For example, in the simulation of the OWC device, the time step would exclusively depend on the velocity that the air acquires when accelerating through the exit orifice of the air chamber (see Figure 1 - right). Hence, in some cases, it can be convenient to use a free surface solver that still advects the air-water interface but that treats it as a moving boundary by deactivating the air phase.

Of course, a two-phase model is more effective for the simulation of energy extraction processes, and allows a more complete characterization, as we need to know the air pressure to evaluate the hydrodynamic efficiency of the OWC device. Anyway, it could be convenient to use a different physical model, that would only take into account the information given by the water phase, but that would allow a much faster simulation.

Discretization algorithm: we have tested a free surface model that uses a collocated mesh scheme [9] (in this case it was easier to handle then the staggered scheme) for the discretization of the Navier-Stokes equation (hence, with the same governing equations proposed for the two phase model) and modifies the procedure by deactivating the air phase and extending the velocity (and pressure) field to a transition region across the interface that will be advected according to the conservative Level Set method. The velocity-pressure coupling is solved by means of the classical fractional step method, expressed by the following two equations:

$$\mathbf{u}^p = \mathbf{u}^n - \Delta t[\nabla \cdot (\mathbf{u}^n \mathbf{u}^n) - \nu \Delta \mathbf{u}^n] \tag{3}$$

$$\mathbf{u}^{n+1} - \mathbf{u}^{p} = -\frac{\Delta t}{\rho}\nabla p^{n+1} \tag{4}$$

to which, the incompressibility constraint is added: $\nabla \cdot \mathbf{u}^{n+1} = 0$; the subscript n indicates the time instant, while p refers to the *predicted* value. The **predictor velocity** is calculated by

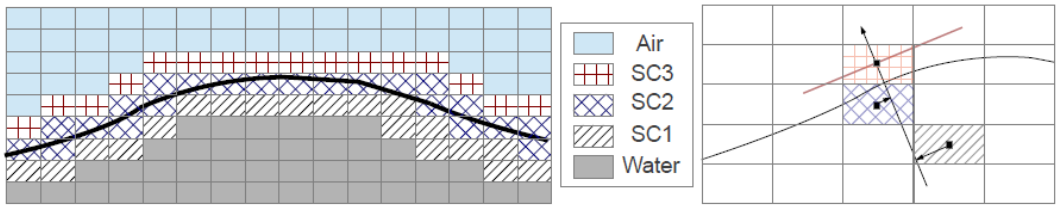

Figure 2: (left) Example of the cell tagging needed for the variable evaluation at the interface between the two phases.(right) Extrapolation scheme: linear interpolation.

integrating Equation (3) on the control volume and applying the divergence theorem to express the fluxes through the CV faces:

$$\mathbf{u}^{p} = \mathbf{u}^{n} - \frac{\Delta t}{V_c}\left[\sum_{f\in F(c)} \phi_f^n \hat{U}_f^n A_f - \nu \sum_{f\in F(c)} (\mathbf{u}_{nb}^n - \mathbf{u}_c^n)\frac{A_f}{\delta d_f}\right] \tag{5}$$

where ϕ_f^n is the convected face velocity, here evaluated according to the upwind scheme, $\hat{U}_f^n$ is the face normal velocity, the subscript c refers to cell values while nb refers to the neighbour cell centroid position; finally, A_f is the face surface and δd_f is the normal-projected distance between cell centroid and neighbour cell centroid. The next step is the resolution of the **pressure field**: divergence is applied to Equation (4), then introducing the incompressibility constraint and applying divergence theorem, it yields the following discrete Poisson equation:

$$\sum_{f\in F(c)} \hat{U}_f^p A_f = \frac{\Delta t}{\rho} \sum_{f\in F(c)} (p_{nb}^{n+1} - p_c^{n+1})\frac{A_f}{\delta d_f} \tag{6}$$

hence, the p^{n+1} field is obtained solving the equation by means of an iterative Preconditionate Conjugate Gradient solver.

Therefore, the pressure is set to 0 in all the points with water fraction (φ) lower than a chosen value between 0 and 1 (eg. $\varphi_{min} = 0.5$) and the cells that crosses the interface are tagged as *state cells*: 1 beyond the interface, 2 across it, 3 to the upper one and so on: an example is showed in Figure 2 - left; the optimal number of interface layers depends on the case that is being simulated. The pressure in the interface region can be now just kept to 0, or smoothed to 0 by extracting the values of the SC1 cells and assigning to SC2 (where p is initially 0) a value taken from the linear interpolation between SC1 and SC3 (where p=0); then, the same process can be applied between SC2 and SC4 to give a pressure to SC3, and so on. These values of pressure

play a role in the calculation of the pressure gradient close to the interface, thus affecting the centered velocity of the *active phase* cells that lies close to the deactivation interface. Anyway, no improvement in the results was noticed when applying the pressure smoothing (compared to the case of keeping 0 pressure at the interface). Next, the **centered velocity** is calculated, by discretizing again Equation (4) over cell the cell when $\varphi > \varphi_{min}$ and deactivating it for $\varphi < \varphi_{min}$:

$$\begin{cases} \mathbf{u}_c^{n+1} = \mathbf{u}_c^p - \frac{\Delta t}{\rho V_c} \sum_{f \in F(c)} p_f^{n+1} \hat{\mathbf{n}} A_f & \text{if } \varphi > \varphi_{min} \\ \mathbf{u}_c^{n+1} = 0 & \text{if } \varphi < \varphi_{min} \end{cases} \tag{7}$$

The final step consists in expanding the velocity field over the interface region. Different criteria can be adopted for the expansion: the simplest one consists in assigning the velocity to the cell center by performing a **weighted average** of the velocities that belongs to the neighboring cells. Another scheme that has been adopted is the interpolation over a line (whose direction must be chosen); in the most general case the line is the one that passes from the considered node and its direction vector is the normal to the interface (calculated as the gradient of φ with the method of the least squares). The interpolation can be linear or higher order, depending on the number of points collected on the line, but not always a higher interpolation order coincide with a better solution, as the shape of the polynomial could be not suitable for modeling a particular profile; moreover, the necessity of collecting points that lies far from the cell, could lead to problems when working on CPU partitions. In the linear case (that does not preserve local maxima), the velocity value for a SC3 cell would be found as:

$$\mathbf{u}_{SC3} = -\frac{|\mathbf{x}_{SC3} - \mathbf{x}_{SC2proj}|}{|\mathbf{x}_{SC2proj} - \mathbf{x}_{SC1proj}|}(\mathbf{u}_{SC1proj} - \mathbf{u}_{SC2proj}) + \mathbf{u}_{SC1proj} \tag{8}$$

where the projected position is found as the intersection of the normal line and its perpendicular plane that passes for the considered cell centroid (SC2 or SC1). The projected velocities are found as:

$$\mathbf{u}_{SCproj} = \mathbf{u}_{SC} + \nabla \mathbf{u} \cdot (\mathbf{x}_{SCproj} - \mathbf{x}_{SC}) \tag{9}$$

where $\mathbf{x}_{SC}$ and $\mathbf{v}_{SC}$ are velocity and position at the cell centroid point. A demostrative example is showed in Figure 2 - right.

3 OWC model

The domain used for the simulations is the one depicted in Figure 1: the solid structure at the right of the domain (including also the right boundary) represents the air chamber; as the waves begin to slam against the front wall of the chamber, its internal water surface begins to obscillate, causing an increase or a decrease of the air pressure inside it. The small orifice allows air to escape the chamber and its function is to mimic the pressure drop that occurs at the turbine inlet nozzle. No-slip boundary conditions are applied to the bottom part of the domain and to the air chamber while Neumann conditions were applied to the other boundaries. The waves are generated by a *wave maker* in a narrow area on the left part of the domain, where a

relaxed numerical solution is applied; the numerical solution and the forcing analytical function are mixed by means of a relaxing function that varies smoothly from 1 to 0 moving from the boundary to the center of the tank $\psi_{relaxed}(\mathbf{x}) = \xi(x)\psi_{analytical}(\mathbf{x}) + (1-\xi(x))\psi_{numerical}(\mathbf{x})$. The wave elevation follows a sinusoidal function that produces progressive waves, identified by the wavelength λ and the amplitude a:

$$\eta(x,t) = a\ sin(\kappa x - \omega t) \tag{10}$$

where $\kappa = \frac{2\pi}{\lambda}$ is the wave number, $\omega = \frac{2\pi}{\tau}$ is the angular frequency and τ is the wave period; these two quantities (κ-ω or λ-τ) are correlated, according to the dispersion relation:

$$\rho_w \omega^2 coth(\kappa h_w) + \rho_a(\omega - \kappa U)^2 coth(\kappa h_a) = (\rho_w - \rho_a) g\kappa \tag{11}$$

where U is the wind velocity. Also the velocity field is imposed in the buffer zone, by means of the analytical solution proposed by Milne [10] for the 2D case. The buffer zone was usually limited to half of the wavelength of the progressive wave, and the domain was built in such a way that the generated waves propagate for three or four times its length before crushing against the front wall of the chamber. The simulation is evaluated by monitoring the evolution of some characterizing parameters as mean surface velocity, air pressure inside the chamber or at the orifice, air flux through the orifice and hydrodynamic efficiency of the OWC device, that can be compared to reference values; it is defined as:

$$\varepsilon = \frac{E_{owc}}{P_{wave}t} \qquad E_{owc} = \int_0^T p(t)q(t)dt = L_{ch}\int_0^T p(t)v(t)dt \tag{12}$$

where P_{wave} is the energy flux of a linear wave across a vertical fluid boundary fixed in space, calculated according to linear wave theory, and E_{owc} is the wave energy per unit depth, where L_{ch} is the chamber length, $p(t)$ is the air pressure in the chamber and $v(t)$ is the mean vertical velocity of the free-surface, deduced from the volume variation of a phase inside the OWC. The maximum energy per meter crest obtainable from a linear wave can be expressed by the following expression:

$$P = \frac{1}{8}\rho_w g a^2 c_g \qquad c_g = \frac{1}{2}\frac{\lambda}{\tau}\left(1 + \frac{4\pi h_w}{\lambda}\frac{1}{sinh(\frac{4\pi h_w}{\lambda})}\right) \tag{13}$$

where the group velocity c_g is given by the linear wave theory for the case of intermediate depth water ($h_w < \frac{1}{2}\lambda$ and $h_w > 0.05\lambda$). Hence, introducing the wave number and the wave frequency definition:

$$P = \frac{\rho_w g a^2 \omega}{8\kappa}\left(1 + \frac{2\kappa h_w}{sinh(2\kappa h_w)}\right) \tag{14}$$

4 Numerical tests

In this section, the numerical model validation is firstly commented; then, the simulations realized both using the accurate two phase model, and the free surface single phase model are reported and commented.

4.1 Model validation: solitary wave

The original two phase Level Set model was firstly validated by simulating the behavior of solitary waves in shallow waters and comparing the results with the analytical data proposed by Mei [11]. The wave was generated by imposing the water elevation on a narrow section of the domain according to the following equation: $\eta(x,t) = a\ sech(\kappa/h_w(x-ct))^2$, where a is the wave peak elevation and h_w is the calm water depth, $c = \sqrt{g(h_w+a)}$ is the wave celerity while the wave number is calculated as: $\kappa = \sqrt{3a/4h_w}$. Good agreement was found between analytical and numerical data, as showed in Figure 3 - left: the wave crest happens to move according to a velocity almost constant and very close to the theorical wave celerity in the whole domain; furthermore, the wave elevation reduces according to the relationship proposed by [11]. The model was assessed to respect the reference also when propagating in shallow waters, where the viscous dissipation is much stronger (Figure 3 - right).

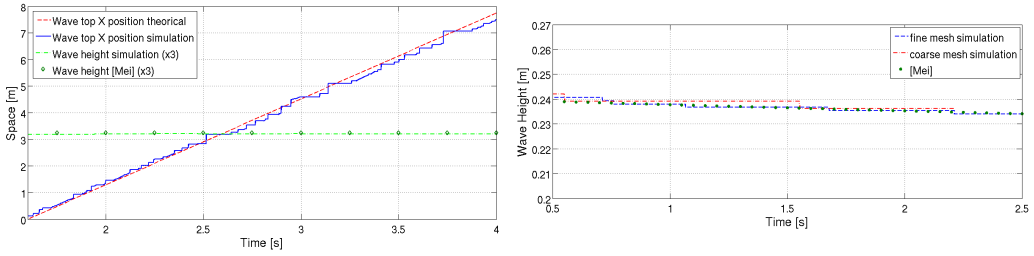

Figure 3: (left) Wave top position and wave height versus time for h_w=0.92 m and a=0.164 m; 300k mesh elements. (right) Wave height versus time for h_w=0.2 m and a=0.037 m; coarse mesh: 70k el., fine mesh: 200k el.

4.2 OWC: two phase model

Large orifice chamber: several tests were carried out on the OWC model. In the first series, the air chamber had a length of 0.64 meters, and the orifice diameter was 2 cm large; the mesh is a cartesian one with 19k elements. The tests were realized generating progressive waves on a large interval of wavelength (from 2.3 to 9 m). Once reached the steady state, the simulations were performed for a number of wave periods sufficient to obtain a statistical value of the hydrodynamic efficiency, and collecting the energy generated over a complete wave period. The collection of data is stopped before that the effect of the reflected waves would affect the solution; on a grid of fixed length, the higher the wavelength of the waves, the shorter the interval in which the collected values are considered reliable (to higher wavelength, coincide higher wave velocity, therefore, also the counter-waves will affect the outcomes in a shorter time). Figure 4 shows the evolution of some typical magnitudes: dynamic air pressure inside the chamber and air flow rate through the orifice. Both air flow rate and pressure peaks rises when increasing the wavelength until $\lambda = 3.7$, while no strong variations are noted by comparing $\lambda = 3.7$ and $\lambda = 4.5$: the pressure peaks obscillates approximately between the same extremes,

with pressure peak values of $\pm 60 Pa$ and maximum air flow rate of $\pm 0.15 m^2/m/s$; finally, a slight reduction of pressure and air flow rate is noted for $\lambda = 7.5$. Such a trend is confirmed by the curve of hydrodynamic efficiency (reported in Figure 5(a)), that shows its maximum for $\lambda = 3.7$ m (where $\overline{\eta}_{OWC} \simeq 30.5\%$).

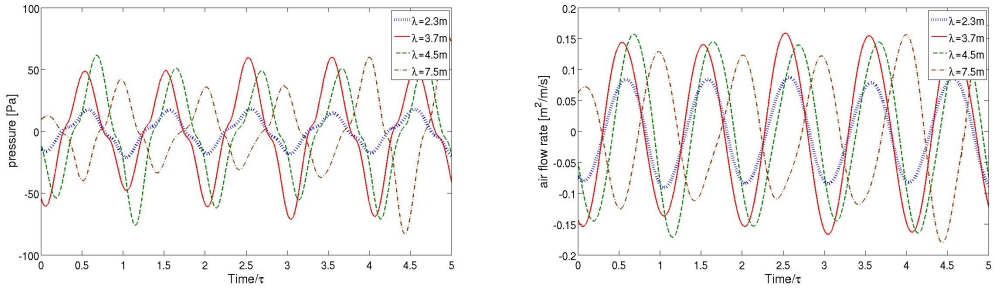

(a) (b)

Figure 4: Air pressure and air flow rate evolution for different λ in an air chamber with a 2 cm large orifice.

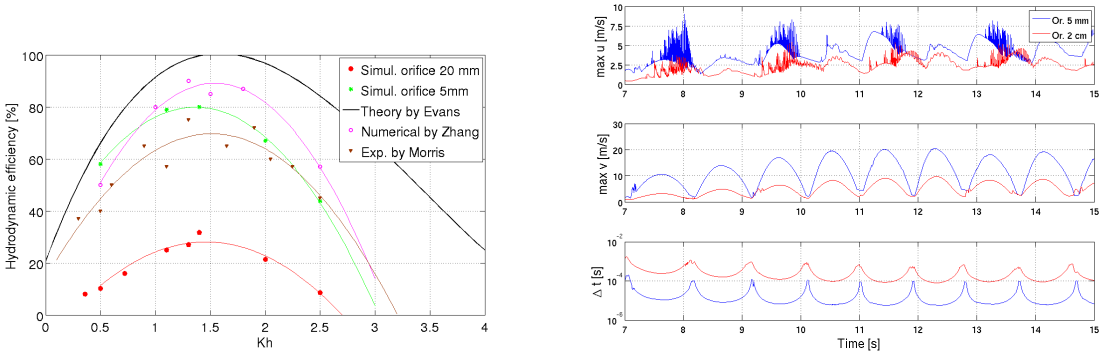

(a) (b)

Figure 5: (a) Hydrodynamic efficiency as a function of the dispersion parameter Kh (defined as $Kh_w = \frac{\omega^2}{g} h_w = \frac{2\pi}{g\tau^2} h_w$), and comparison with some references. (b) Comparison of time step and maximum horizontal and vertical velocities between two simulations carried out with the same λ, but different diameter orifice.

Narrow hole chamber: successively, we realized a new series of tests using a different geometry: the air chamber has the same width (0.64 m) but the orifice is narrower (5mm diameter), with the aim of obtaining an increase of the efficiency. The mesh is much finer than in the past analysis (64k vs 19k elements), expecially around the orifice. Five tests were realized, varying λ from 2.3 to 7.5 m. In Figure 6 the evolution of the significant magnitudes is plotted. Again,

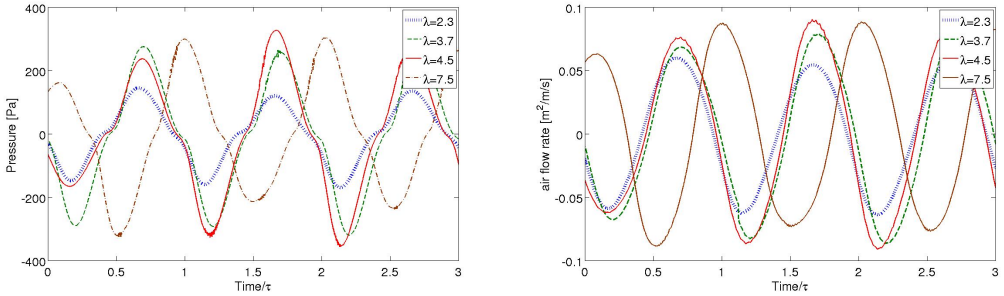

(a) (b)

Figure 6: Air pressure and air flow rate evolution for different λ in an air chamber with a 5 mm large orifice.

it is possible to notice that the highest peaks (for air chamber pressure and air flow rate) are reached for the intermediate wavelengths of the scale ($\lambda = 3.7$ and $\lambda = 4.5$), reflecting the behaviour that was showed in the past series of experiments, and furthermore showing a much more closer value of mean efficiency in the two best cases ($\overline{\eta}_{\lambda=3.7} \simeq 80\%$ vs $\overline{\eta}_{\lambda=4.5} \simeq 78.9\%$). The reduction is not so marked instead for the highest wavelength ($\lambda = 7.5$), thus leading to almost comparable values of the absorbed power (showed in Figure 8(a)). The values of efficiency (fitted by means of a second degree polynomial) are plotted again in Figure 5(a), where experimental data are compared with some references: the upper limit is consituted by the theorical efficiency obtained by Evans [2]; in the intermediate interval of Kh, our fitting lies in the middle of the numerical data obtained by Zhang [4] and the experimental ones obtained by Morris [3], while it shows slightly higher values for the highest wavelengths and slightly lower values for the shortest ones. Anyway, the overall behavior agrees with the experimental data.

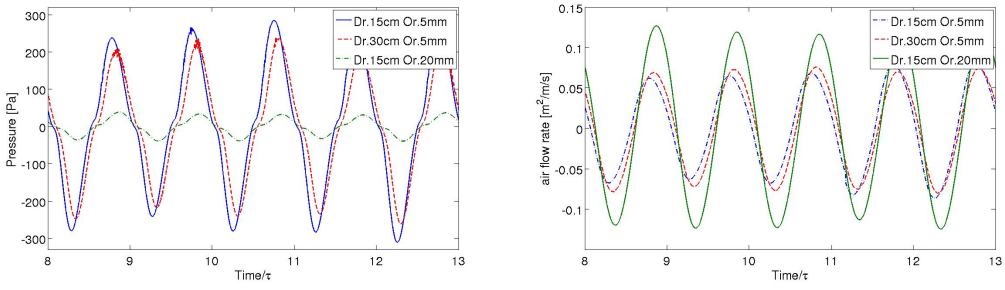

(a) (b)

Figure 7: Air pressure and air flow rate through the orifice varying some geometrical parameters ($\lambda = 3.7$). Dr. (draught) refers to the immersion depth of the front wall; Or. refers to the diameter of the orifice.

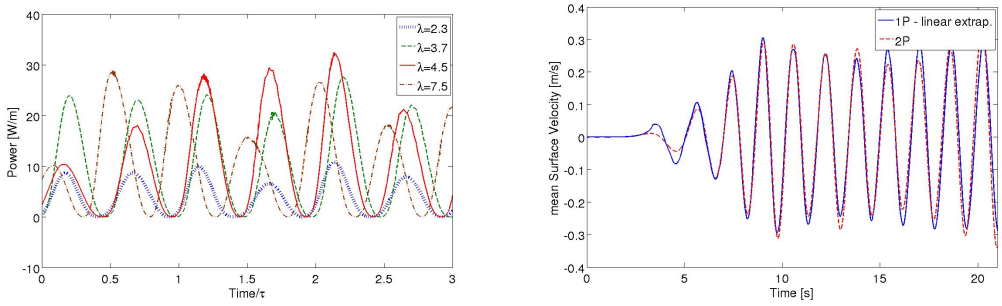

(a) (b)

Figure 8: (a) Extracted power (per unit depth) evolution for different λ in an air chamber with a 5 mm large orifice. (b) Mean vertical velocity of a limited section of water, 1P vs. 2P model comparison.

Comparison between configurations: reducing the orifice diameter led to an increase of the efficiency, due to the higher vortex formation inside the chamber and the strong increase of the dynamic component of the air pressure; on the other side, the air flow rate decreases consistently, as the water surface motion results confined by the higher air pressure (an example in showed in Figure 7). From a numerical point of view, the reduction of the orifice diameter has a strong influence on the computational time of the simulation, due to the important increase of the vertical velocity of the air through the hole (as showed in the central plot of Figure 5(b)) and the consequent necessity of reducing considerably the mesh size in this zone of the domain; both this factors causes a reduction of the time step, calculated according to the CFL criteria (as showed in the bottom plot of Figure 5(b)). The OWC device can be also optimized in terms of wall thickness, front wall draught, air chamber width and so on; given λ, we increased the immersion depth from 15 to 30 cm, obtaining a reduction of the efficiency, that passes from $\overline{\eta} \simeq 0.8$ to $\overline{\eta} \simeq 0.67$ (due to a mean pressure gap of 30-40 Pa, see Figure 7). As introduced by Evans [2], the *resonance* period is: $T_r = 2\pi\sqrt{D/g}$ where D indicates the draught of the air chamber; it confirms that the resonance period rises when increasing the wall depth.

4.3 OWC: single phase model

The model was firstly tested by simulating the unbounded movement of water when agitated by progressive waves; Figure 8(b) shows the evolution of the free surface velocity of a small sector of water far from the wave maker zone, obtained with the two phases (2P) and the single phase (1P) model using a linear extrapolation of the velocity field. The 1P model shows a very close behaviour to the 2P one, even considering the limits of the simple field expansion technique. Hence, some tests were realized on the OWC device ($d_{orifice} = 2cm$): as showed in Figure 9(a), good agreement was found between the velocity of water inside the air chamber calculated by the two models. As we do not have informations about the air phase, we suppose that the air flow rate (per unit depth) generated by the free surface motion is equal to the flow rate through the orifice: $Q(t) = L_{owc}\bar{v}_{owc}(t) = d_{or}\bar{v}_{or}(t)$, where L_{owc} is the chamber width, v_{owc} is the mean vertical velocity of the water inside the chamber, $d_{orifice}$ is the diameter of the orifice and

v_{or} is the mean vertical velocity of the air through the orifice. The pressure drop is evaluated by

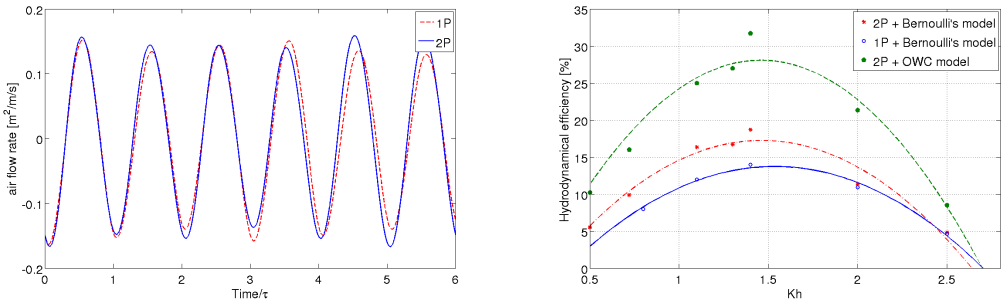

(a) (b)

Figure 9: (a) Air flow rate comparison between 1P and 2P simulations ($\lambda_{\text{wave}} = 3.7$). (b) Hydrodynamical efficiency comparison between the two series of test, realized over OWC chamber with $d_{orifice} = 2cm$.

applying the Bernoulli's equation between the inlet of the orifice and the environment, therefore the power extracted is $P(t) = \Delta p(t)Q(t)$ where $\Delta p(t) = \frac{1}{2}\rho_a \bar{v}_{or}^2(t)$ [12]. In Figure 9(b) is showed the curve of efficiency obtained with 1P and 2P (both with the OWC model and the Bernoulli's one) simulations: the curves realized with the Bernoulli's model are quite in agreement but rather lower than the one realized with the 2P+OWC model scheme, as we are not considering the added dynamic component of the air pressure inside the air chamber. The mesh must be finer than in the case of 2P (37k vs 19k elements), to ensure that the extrapolation leads to consistent values of velocity. Nevertheless, the computational time results consistently reduced ($\sim 60\%$) and due to the proportionality of the models, the 1P scheme could be useful to perform some parametrical analysis.

5 Conclusions

A conservative Level Set method was used to simulate the behaviour of an air-water system that manage to extract energy from the ocean wave motion (Oscillating water column system). Good agreement was found between the results (mainly referring to the hydrodynamical efficiency of the device) and some experimental and numerical references; moreover, we demostrated the capability of our model to adapt to different geometrical configurations and environmental conditions, that will be analyzed in future works (different configuration of the domain, multiple waves generation). In the second part of the work, we simulated the same test case using a single phase Level Set method; on the one side, we obtained velocity and pressure fields that mimics quite accurately the behaviour of the free surface motion, even if more efforts must be done in the expansion of the velocity field, using more comlex extrapolation schemes that could allow the simulation of a wider range of single phase problems. On the other side, we noticed that the simple model that we used to characterize the power output was not precise enough, even if it offers a good proportionality to the reference data and it is much faster.

Hence, some more efforts will be done to improve the reliability of the model.

6 Aknowledgments

This work has been financially supported by the Ministerio de Economìa y Competitividad, Secretarìa de Estado de Investigacìon, Desarrollo e Innovacìon, Spain (ENE-2010-17801 and ENE-2011-28699), a FI Grant by AGAUR (Generalitat de Catalunya) and by Termo Fluids S.L.

REFERENCES

[1] SI Ocean, Ocean energy: state of the art, Online report, December 2012.

[2] Evans, D.V., Porter, R., Hydrodynamic characteristics of an oscillating waters column device, *Appl. Ocean. Res.*, Vol. 17, pp 155-164, 1995.

[3] Morris-Thomas et al., An investigation into the hydrodynamic efficiency of an oscillating water column, *J. Offshore Mech. Arct. Eng.*, 129 (2007), pp. 273–278.

[4] Zhang Y. et al., Air–water two-phase flow modelling of hydrodynamic performance of an oscillating water column device, *Renewable Energy*, Volume 41, May 2012, Pages 159-170.

[5] Teixeira P. et al., Numerical simulation of an oscillating water column device using a code based on Navier–Stokes equations, *Energy*, Volume 61, 1 November 2013, Pages 513-530.

[6] Lv X. et al., A novel coupled level set and volume of fluid method for sharp interface capturing on 3D tetrahedral grids, *Journal of Computational Physics*, Volume 229, Issue 7, 1 April 2010, 2573-2604.

[7] Carrica et al., An unsteady single-phase level set method for viscous free surface flows. *Int. J. Numer. Meth. Fluids*, 53: 229–256 (2007).

[8] Balcázar N. et al., A Finite-Volume/Level-Set Method for Simulating Two-Phase Flows on Unstructured Grids. Submitted to the *International Journal of Multiphase Flow*.

[9] Jofre L. et al., Conservation Properties of Unstructured Finite-Volume Mesh Schemes for the Navier-Stokes Equations, *Numerical Heat Transfer*, Part B, 65:53–79, 2014.

[10] Milne-Thomson LM, *Theoretical Hydrodynamics*, Dover publications, 1994.

[11] Mei, C.C., *The applied dynamics of ocean surface waves*. Wiley, New York, 1983.

[12] Sheng W. et al., On wave energy extraction of oscillating water column device. Submitted on 4^{th} *International Conference on Ocean Energy*, October 2012.